Progress in Additive Manufacturing
https://doi.org/10.1007/s40964-025-01123-3

RESEARCH

A methodical approach for the integration of foil-type strain gauges in PBF-LB/M components

Thomas Bareth[1,2] · Niklas Fromm[1,3] · Maja Lehmann[1] · Georg Schlick[1] · Christian Seidel[3]

Received: 13 January 2025 / Accepted: 12 April 2025

Abstract
Powder bed fusion of metals using a laser beam (PBF-LB/M) enables the production of smart components by facilitating the integration of sensors almost anywhere within a part through its layer-by-layer manufacturing process. This allows for sensor placement near critical points of interest while providing protection against environmental influences. This study introduces a novel methodology for integrating bonded linear foil strain gauges within PBF-LB/M components—an approach not previously explored. The objective was to achieve reproducible in-situ monitoring of strain loads in components, with strain gauges integrated flexibly and cost-effectively during the PBF-LB/M process. Key steps included assessing the temperature at the integration position, selecting a suitable adhesive, preparing the bonding surface to optimize adhesion, designing appropriate cavities for sensors and wiring, and establishing guidelines for manual integration of the strain gauge within the PBF-LB/M environment. The feasibility of this integration methodology was successfully validated through strain measurements obtained from tensile tests on a sample with an integrated strain gauge. The measurement signal demonstrated a faithful measurement of strain and exhibited minimal deviations between repeated measurements.

Keywords Condition monitoring · Smart parts · Sensor integration · Additive manufacturing · Powder bed fusion of metals using a laser beam (PBF-LB/M)

1 Introduction

1.1 Motivation

Predictive maintenance and condition monitoring are rapidly developing trends in industrial services. In 2022, 81% of surveyed companies reported investing time and resources to enhance their predictive maintenance strategies [1]. The global predictive maintenance market was estimated at USD 7.85 billion in 2022 and is projected to grow at a compound annual growth rate (CAGR) of 29.5% from 2023 to 2030, reaching USD 60.13 billion by 2030 [2].

This trend puts pressure on the manufacturing sector to produce components equipped with sensors, enabling in-situ condition monitoring [3].

For instance, the use of lithium-ion batteries (LIBs) in electric vehicles (EVs) requires accurate estimation of the battery's state to ensure safe and efficient control, monitoring, and optimization. Condition monitoring facilitates the collection of measurement data and allows for immediate action if significant changes in the state or condition of the battery are detected. Critical condition parameters include temperature variations or expansion of the cell housing, which may occur due to increased internal pressure and could potentially cause damage to the cell or its surroundings [4, 5]. Data from condition monitoring of battery cells can be used to evaluate cell quality in detail, validate simulations, and train artificial intelligence (AI) models, supporting

✉ Thomas Bareth
thomas.bareth@igcv.fraunhofer.de

Niklas Fromm
niklas.fromm@igcv.fraunhofer.de

Maja Lehmann
maja.lehmann@igcv.fraunhofer.de

Georg Schlick
georg.schlick@igcv.fraunhofer.de

Christian Seidel
christian.seidel@hm.edu

[1] Fraunhofer Institute for Casting, Composite and Processing Technology IGCV, Augsburg, Germany

[2] Technical University of Munich, Munich, Germany

[3] Munich University of Applied Sciences, Munich, Germany

Published online: 05 June 2025

new cell developments and allowing for more efficient definition and validation of cell concepts [6]. In most electrochemical energy storage systems, direct measurement of internal battery states is not possible due to the chemically aggressive environment within the electrolyte liquid, requiring indirect estimation of these states [4]. Under severe or extreme operating conditions, the highly nonlinear relationship between internal states and externally measured signals poses a significant challenge [4, 7]. Integrating sensors into the battery cell housing offers the potential for more accurate and faster-response signals without affecting the cell chemistry [8].

Additive manufacturing (AM) processes, such as powder bed fusion of metals using a laser beam (PBF-LB/M), offer this opportunity to integrate sensors directly within components at specific points of interest, enabling encapsulated cavity designs tailored to the sensor's geometry [9, 10]. By integrating sensors during the part build-up, they can be positioned almost anywhere within the part due to the layer-by-layer nature of AM. For PBF-LB/M, the process runs until reaching a specified height, where it is interrupted. The sensor is then placed into a designated cavity and the process resumes. This integration method allows sensors to be embedded without dividing the component into multiple parts, making it possible to create smart components with minimal impact on their overall properties [10, 11]. This study addresses a gap in existing research by presenting a novel methodology for integrating non-weldable foil strain gauges (SGs) into components produced via PBF-LB/M, an approach that has not been previously explored. The aim is to enable in-situ monitoring of strain loads within the component, as close as possible to the point of interest while providing protection for the SG against environmental influences. This approach holds significant potential for industrially relevant smart part applications.

1.2 Literature review

In previous research, various types of strain-measuring sensors have been integrated during PBF-LB/M. Numerous studies have focused on the integration of fiber Bragg gratings (FBGs) [12–14]. In all of these studies, metallic jacketed FBGs were used to protect the fibers from the high thermal energy input of the laser [12–14]. This jacket is required to serve as a thermal barrier that can absorb the huge energy input of the laser during the process. Connecting the jacket to the AM part proved challenging for different research groups [12, 13, 13]. The high temperature necessary for welding the metallic jacket of the FBG to the AM part (> 430 °C) [14] could loosen the connection between the casing and the fiber so that no force transmission and thus no reliable detection of forces or temperatures was possible [10]. Stoll et al. [12] achieved acceptable results for temperature measurement, though the bonding quality between the FBG and the measurement object was insufficient for reliable strain measurements. Since the integration of FBGs is challenging in the PBF-LB/M process, the integration is often done after the build job completion. Typical methods include the design of a drop-shaped cavity at the position of integration, where the FBG can be inserted and attached using bonding agents, or leaving a cavity for a carrier plate on which the FBG is mounted on [15]. FBGs can be integrated into very thin parts and confined spaces due to their small diameter [14]. However, the integration position must remain accessible in the finished part.

In addition to FBGs, other research efforts have investigated the integration of strain-measuring sensors during AM using weldable SGs [10, 16, 17]. Binder et al. [16] examined the manual integration of weldable SGs during PBF-LB/M. A weldable SG was placed into a cavity during a process interruption. After placing the sensor, it was welded to a tensile rod using the laser of the PBF-LB/M system before resuming the process. Selecting the appropriate welding parameters proved challenging and likely requires extensive study for different material combinations. The integrated SG was tested through tensile tests and demonstrated its effectiveness in measuring the load on the tensile rod [16]. Binder et al. [18] also examined the automatic integration of weldable SGs. They used a kinematic system to remove the powder and to place the sensor. They observed unwanted bending in the steel plate on which the weldable SG was mounted. In their study, an X8Cr17 (1.4016) SG carrier plate was welded to AlSi10Mg tensile rods. The carrier plate of the inserted SG deformed due to thermally induced stresses, causing it to protrude into the engagement range of the powder recoater [18]. Depending on the extent of this deformation, it could lead to a failed build job or even damage to the powder recoater [10]. This deformation is caused by heat build-up in the carrier plate, which can be mitigated by using an adapted exposure strategy [10, 18]. Compared to FBGs, SGs generally require larger cavities. Since the cavity for SGs is not drop shaped, the rectangular design necessitates a"roof" above the sensor, as overhangs in PBF-LB/M parts either require support structures or must be tapered for manufacturability. Dani [17] integrated weldable SGs. These SGs were manually integrated using a similar approach to that of Binder et al. [18], though the significantly smaller size of the cylindrical SG geometry required a smaller cavity design. However, no data on the measurement accuracy of the integrated SG is provided [17].

1.3 Problem statement and approach

The literature review highlights that existing solutions for integrating strain-measuring sensors in PBF-LB/M components have certain drawbacks. These downsides,

particularly regarding ease of integration, size requirements, design flexibility, and integration costs for FBGs and weldable SGs, are evident [10, 12–14, 16, 17]. Non-weldable SGs attached with adhesives present a promising solution due to their ease of integration using conventional methods, significantly lower costs, and their smaller size in contrast to weldable SGs. Non-weldable SGs attached with adhesives are typically much more affordable compared to weldable SGs and FBGs. Their cost is usually about 5 to 10 times lower than that of weldable SGs. When compared to FBGs, the difference is even greater, as FBGs can be over 15 times more expensive than non-weldable adhesive-based SGs. These advantages highlight the need for a flexible integration method for non-weldable SGs using adhesive bonding in PBF-LB/M components. At the time of this study, no established method or proof of feasibility existed for integrating non-weldable SGs into PBF-LB/M components via adhesive bonding. Developing a reliable manual integration approach for these inexpensive and widely available SGs presents a valuable scientific opportunity. A well-defined method with clear, step-by-step guidance could minimize errors commonly associated with manual handling. Given the widespread adoption of AM for small batch size production, manual integration of non-weldable SGs offers a cost-effective alternative requiring minimal additional hardware compared to automated integration methods.

However, the conditions during PBF-LB/M pose significant challenges for non-weldable SG integration. Standard SG installation methods need adjustments since the sensor integration occurs inside the PBF-LB/M build chamber. For instance, the temperatures during the process, which depend on the powder material used, can be too extreme for certain sensors or adhesives [10, 19, 20]. The melting temperatures of relevant metals range from 660 °C for aluminum to 3,422 °C for tungsten [10]. Beyond localized high temperatures from laser energy input, the build plate is often heated to reduce thermal distortion [21]. For aluminum alloys like AlSi10Mg, maintaining a build plate temperature of 160 °C is recommended for minimizing thermal stresses and distortion [22]. Many bonding agents for non-weldable SGs are not suitable for high temperatures or require long curing times and constant pressure during curing. The polyimide carrier foil and the soft solder in non-weldable SGs generally exhibit lower heat resistance than the materials found in weldable SGs [23]. The limited accessibility within a PBF-LB/M system further complicates the integration process. Sandblasting a component's bonding surface within the build chamber is difficult without modifications to the PBF-LB/M system, making it impractical with commercially available machines. Other factors like inert gas flow and potential powder contamination from electrically conductive metallic particles must also be considered.

A feasibility study is essential to verify whether the thermal conditions at the position of integration during the PBF-LB/M process permit the use of adhesives and non-weldable SGs. While the basic integration steps for sensors are available from Binder [16], the integration of non-weldable SGs is not yet possible with the current state of the art.To demonstrate that such integration during PBF-LB/M is feasible, several research questions and challenges must be addressed. These include the selection and application of suitable adhesives, the temperature resistance of components, surface preparation for bonding, and the design of SGs and wire cavities under PBF-LB/M process conditions. Accordingly, the following research approach investigates the hypothesis that the integration of non-weldable SGs during the PBF-LB/M build process is feasible through the development of an appropriate enabling methodology.

2 Materials and equipment

As PBF-LB/M manufacturing system, an EOS M290 (EOS GmbH, Krailling, Germany) was used. Pure aluminum powder (PureAl; m4p GmbH, Feistritz i.R., Austria) was chosen, as it closely matches the aluminum typically taken in conventionally manufactured battery cell housings, which is an intended use case for this research. The laser parameter for fabrication included a volumetric energy density (VED) of 38.82 J mm^{-3}. Unless otherwise specified, SG in the following refers to non-weldable foil-type strain gauges bonded with an adhesive. The SG 3/350 CLY43-3L-1 M (HBK GmbH, Darmstadt, Germany) illustrated in Fig. 1, was chosen to demonstrate the methodical approach because its commonly used design makes it representative of a broad range of measurement applications [24]. The SG itself has an operating temperature range of ± 200 °C, with a thermal expansion coefficient matching that of aluminum ($\alpha = 23 \times 10^{-6}\ K^{-1}$). It comes pre-wired with

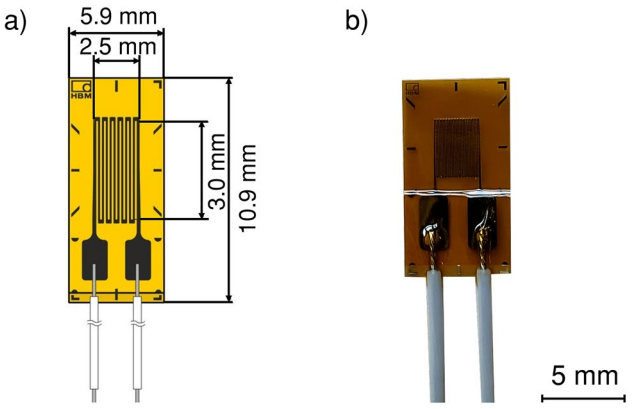

Fig. 1 (**a**) Schematic view with geometry specifications [25], and (**b**) corresponding SG

50 mm long fluorinated ethylene propylene (FEP) wires, which are soldered to the SG and can withstand temperatures of up to 180 °C. These wires in turn are soldered to a 1.0 m long thermoplastic elastomer (TPE) ribbon cable, capable of resisting temperatures of up to 150 °C [25].

To ensure that the SG and its wires can withstand the PBF-LB/M process, an initial understanding of the process temperature under specific conditions, including the manufacturing system, selected laser parameters, and powder material at the integration site, was developed. A PT100 resistance thermometer (Hotset GmbH, Luedenscheid, Germany) was integrated into a test sample to collect data on the temperatures occurring. For this initial test, the build plate heating was set to 60 °C. The resistance thermometer was positioned at the location where the SG's measurement grid would be placed during integration. It was clamped in the cavity, eliminating the need for adhesive or bonding agents for fixation. By connecting the resistance thermometer to an MCR-4TC (T&D Corporation, Matsumoto, Japan) data logger the temperature data after the build job resumption was recorded.

The initial step in assessing the success of the SG integration methodology involved ensuring a fault-free installation. This was done by measuring the electrical resistance of the SG and confirming that there were no ground faults between the SG and the AM component. If the resistance of the SG deviated from its datasheet specification ($350 \pm 0.5\%$ Ω for the SG 3/350 CLY43-3L-1 M), it indicated potential damage to the SG or its wiring, rendering the integration unsuccessful. Besides that, HBK specifies that resistances below 100 MΩ between the SG and its measurement object are inadequate for a proper SG installation [24]. Such ground faults can degrade the quality of the measurement signal, resulting in anything from completely unusable data to a significant increase in signal noise. Given that conventional multimeters, like those employed in this study, have a maximum measurement range of 60 MΩ, installations exceeding this value and exhibiting no unusual measurement behavior are considered to be successful and free of ground faults. To evaluate the measurement characteristics of the integrated SG, a tensile sample with an encapsulated SG was manufactured (see Fig. 2). After the AM process, the tensile sample was removed from the build plate using a diamond wire saw (DWS.375E, Diamond WireTec GmbH & Co.KG, Weinheim, Germany) and machined by milling to achieve a uniform sample thickness.

3 Integration methodology

This section presents the experimental findings, evaluations, and guidelines for each critical step involved in integrating SGs into PBF-LB/M parts. These steps are divided into assessing the temperature at the position of integration, the selection of an adhesive, the design of the SG and wire cavities, the position of integration and process interruption, the actual SG integration, and the procedure to restart the build job.

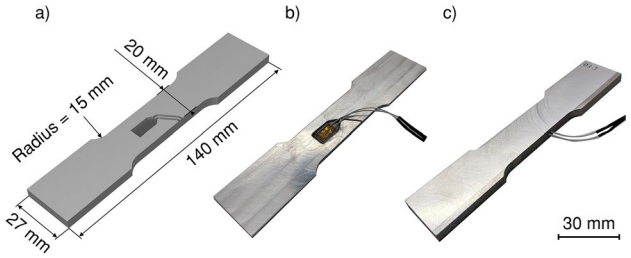

Fig. 2 (**a**) Schematic representation of the sectioned tensile sample with geometry specifications, (**b**) milled cross-sectional view illustrating the SG integration position, and c) milled PBF-LB/M manufactured tensile sample with integrated SG

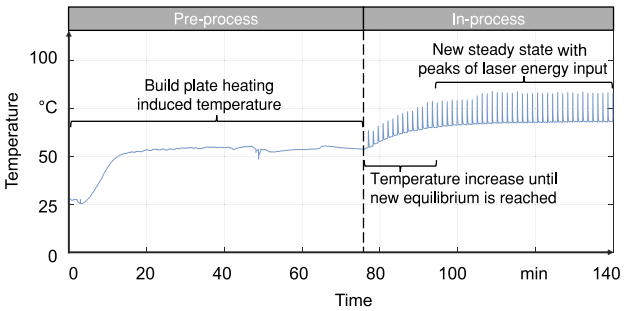

Fig. 3 Process temperature at the position of integration with 60 °C build plate heating measured by a resistance thermometer

3.1 Temperature at the position of integration

Figure 3 shows the temperature data recorded by the resistance thermometer integrated into a test sample. The graph illustrates the measured temperature as a function of time throughout the duration of the build job. The process temperature is primarily influenced by the build plate heating and the thermal peaks, which represent the energy introduced by the laser for solidifying each layer above the layer of interruption and measurement.

A "steady state" temperature was achieved 18 min after the process resumed. The highest recorded temperature peak reached 83 °C, while the minimum temperature throughout the steady state was 69 °C. Since the thermometer is placed at the location corresponding to the SGs measurement grid, it is positioned at a distance from the laser's local energy input. As a result, the recorded temperature peaks are lower than those reported in other studies investigating process temperatures during PBF-LB/M [26]. This temperature

measurement represents an important first step for characterizing the thermal environment at the integration site, indicating and evaluating the ability of the SGs, their wiring, and the adhesive to endure the temperatures present during the PBF-LB/M process.

3.2 Selection of adhesive

Bonding agents are required to fixate SGs to their measurement object and to transfer the strain in that object as faithful and with as little loss as possible [20]. Several types of adhesives were considered of interest for the integration of SGs in PBF-LB/M parts. To determine the most suitable adhesive for the SG bonding, a utility analysis was conducted, examining two different cyanoacrylate adhesives, one methylacrylate adhesive, and one hot- and one cold-curing epoxy resin. The evaluation criteria included ease of handling, ease of integration, temperature range, curing time, and the longevity of the adhesive. Table 1 presents the results of the utility analysis and summarizes the general differences among the adhesive types examined. The most important factor is the ease of integration, since fault-free, reproducible sensor integration should be achieved within a PBF-LB/M system. The second most important factor is the temperature range of the adhesive since the adhesive must withstand the PBF-LB/M process temperatures after the integration. Lastly, the ease of handling and the curing time are weighted the lowest, though they are still important criteria.

Notably, the longevity of bonding agents is difficult to evaluate on its own, since it is dependent on the installation as a whole, as well as the environmental circumstances [19, 20, 27]. The ease of handling includes the number of components of an adhesive, their pot life and necessary tools and preparation steps. An adhesive that is easy to handle reduces possible sources of error. A low curing time is ideal, to decrease the required time to perform a sensor integration (and thus the time of process interruption). A short as possible curing time leads to a more economical sensor integration.

The majority of experimental SG installations use cyanoacrylate adhesives. Commonly referred to as super glue, cyanoacrylates are fast polymerizing cold-curing one-component adhesives. They generally have low viscosity and are easy to apply on horizontal surfaces. Under thumb pressure, the adhesive hardens in less than a minute, forming a very thin layer of less than 10 µm. A notable advantage of these adhesives is their compatibility with a wide range of metals and plastics. Cyanoacrylates only cure on smooth surfaces (2–4 µm), meaning that rougher surfaces (> 4 µm) should be avoided [20]. Methylacrylates are cold-curing, two-component adhesives typically composed of a liquid and a powder that are mixed before application, producing a"stringy" consistency. Key advantages include their applicability to a wide range of structural materials, a fast measuring readiness, and an easy installation. Methylacrylates generally fully cure in 30 min in layer thicknesses of about 60 µm. Epoxy resins are also two-component adhesives, but can be cold- or hot-curing. They consist of a resin component and a hardener, that causes the liquid to polymerize. The exact properties of epoxy resins depend on the resin and hardener used. Compared to cyanoacrylates and methylacrylates, generally, epoxy resins possess higher application temperatures and better long-term stability. The trade-off is a time-consuming installation, that often requires curing at elevated temperatures in a furnace, as well as the application of contact pressure for at least several minutes or even up to a few hours [19, 20].

Generally, cyanoacrylates are recommended to be used for experimental stress analysis only, while epoxy resins are recommended for long-term transducer manufacture [19]. Still, SG installations using cyanoacrylate adhesives can theoretically last for decades, if they are sufficiently protected from the environment and especially moisture [27].

The biggest drawback of using cyanoacrylates is the comparatively low longevity of the installed SG. Under ambient indoor conditions, cyanoacrylate bonds can often show no significant change in strength over a period of years. In contrast, epoxy resins can last for over 30 years [27]. Over time, cyanoacrylates tend to show zero-point drift, which is challenging for longer zero-point-related measurements. This is caused by moisture, which can creep between the carrier foil of the SG and the adhesive [20]. Both the longevity of the cyanoacrylate bond and the quantitative size of the zero-point drift depend on the environmental conditions and the SG installation and its protections. Notably, this drift is

Table 1 Comparison between different adhesive types and their suitability for the integration of SG in PBF-LB/M parts ranging from disadvantageous (−) to highly advantageous (+++)

Evaluation Criterion	Cyanoacrylate	Methylacrylate	Epoxy resin
Curing Time	+++	+++	-
Ease of handling	+++	++	+
Ease of integration	+++	++	-
Longevity	-	+	+++
Temperature range	+	-	+++

of no importance for non-zero point-related measurements, since it occurs over a long time (weeks to months). Zeroing the sensor is a reliable method of compensation for this drift [20]. By having the sensor encapsulated in a cavity, it is well protected against the environment and mechanical harm. By closing the gap between the wire and the wire cavity (e.g., by filling it with epoxy resin), the SG installation can be sealed. This not only shields the SG from environmental influences but also provides strain relief for the wires. Such measures enhance the longevity of the SG and adhesive by preventing mechanical damage and minimizing exposure to moisture [20].

Cyanoacrylate adhesives generally have higher operating temperature ranges and glass transition temperatures than methylacrylates. The cyanoacrylates examined for this study and in preliminary tests (CA-80 by HBK GmbH, Darmstadt, Germany and CC-33A by Kyowa Electronic Instruments CO., LTD, Tokyo, Japan) possess a maximum operating temperature of 120 °C, compared to 50 °C for the methylacrylate (X60 by HBK GmbH). In this context, epoxy resins are beneficial due to their high operating temperature of up to 200–315 °C (X280 and EP310 by HBK GmbH). Depending on the type of epoxy resin used, they either require high curing temperatures in an oven, which is challenging without removing the build plate from the PBF-LB/M system, or relatively high constant mechanical pressure for up to a few hours. Curing times for these resins range from one to 36 h, depending on the temperature. During this time, the PBF-LB/M process is paused, significantly reducing its economic efficiency. Based on this comprehensive comparison of different adhesives for SG integration, the cyanoacrylate CC-33A was selected as the most suitable for the SG integration methodology. It has an operational temperature range of up to 120 °C and a glass transition temperature of 150 °C. This ensures that the cyanoacrylate can withstand process temperatures up to 150 °C and effectively transfer strain to the SG without degradation under operating conditions up to 120 °C.

3.3 Design of the cavity

The size of the SG defines the overall dimensions and shape of the sensor cavity. A key requirement for the cavity design is that the sensor cavity should be as compact as possible to minimize the necessary design space while maintaining the sensor's measurement accuracy and ensuring reliable and repeatable integration. Furthermore, the SG cavity must not compromise the structural integrity of the part, preventing mechanical failure due to an excessively large cavity. The wire cavity should provide a pathway for the wires to exit the part, remain compact to allow for sealing by filling the gaps between the wires and the cavity, yet be large enough to protect the wires from damage during the PBF-LB/M process and ensure consistent and reliable wire positioning.

For the sensor cavity, a rectangular design with a roof was adapted from Binder et al. [16], who successfully integrated a weldable SG. This design was modified by incorporating a tapered extension at the front of the cavity to improve the handling of wires attached to the SG. Additionally, the wire cavity was further refined.

The sensor cavity geometry is systematically described by dividing it into two sections: the lower rectangular portion, termed the knee cavity, and the upper angled portion, called the roof cavity. Binder et al. [16] defined the cavity size by adding a 0.3 mm clearance to both the sensor's length and width, ensuring precise placement while accounting for PBF-LB/M tolerances. Figure 4a illustrates this concept, showing the division into a knee and roof cavity, while Fig. 4b depicts the placement of the SG within the cavity.

Figure 5 and Table 2 present the final geometric parameters for the sensor and wire cavity design. Comprehensive testing demonstrated that clearances c_{Cavity} greater than 0.3 mm did not affect the signal quality of the integrated SG but resulted in a significant increase in sensor cavity volume. Therefore, a clearance of 0.3 mm was identified as optimal for achieving a compact and reliable SG integration, along with a wire cavity height of h_{E} of 0.9 mm.

Furthermore, the tests revealed that roof angles β below 20° lead to asymmetrical layer buildup in unsupported roof geometries under the specified process parameters. Consequently, a minimum roof angle β of 20° was chosen. The knee cavity height is determined by the SG height of approximately 0.7 mm, which includes its wires and soldering points. To account for thermal shrinkage and manufacturing tolerances, the cavity height was adjusted to a minimum h_{k} of 1.0 mm. For cyanoacrylate adhesives, achieving a low surface roughness S_{A} of 2–4 µm is crucial to ensure a sufficient transfer of strain from the measurement object to the SG.

PureAl samples analyzed in preliminary tests had a surface area roughness S_{A} of 30 µm after manufacturing with the process parameters used in this study. To examine if the surface roughness could be improved, remelting tests were

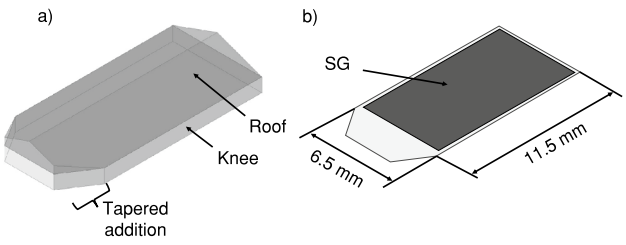

Fig. 4 Schematic view of the sensor cavity with: (**a**) the separation in a roof and a knee cavity, and (**b**) the position of the SG inside the cavity

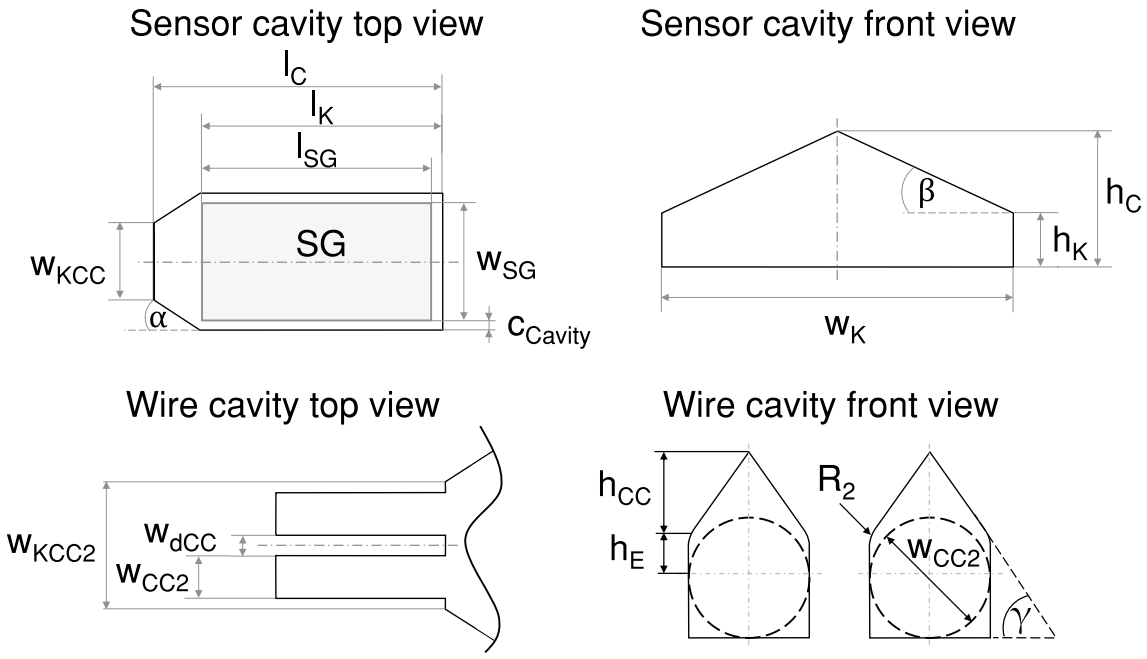

Fig. 5 Geometric variables (described in Table 2) for the design of the sensor and wire cavity

Table 2 Recommended geometric variables for the design of the sensor and wire cavities, with dimensions derived from the SG 3/350 CLY43-3L-1 M at the marked positions (*)

Variable	Description	Variable
α	taper angle	$\alpha = 33°$
β	roof angle	$\beta = 20°$
γ	wire cavity roof angle	$\gamma = 55°$
d_{wire}	diameter of wire	$d_{\text{wire}} = 0.60$ mm *
h_C	sensor cavity height	$h_C = h_K + \frac{w_K \times \tan\beta}{2}$
h_{CC}	wire cavity height	$h_{CC} = 1.8$ mm
h_E	wire cavity height extension	$h_E = 0.9$ mm
h_K	knee cavity height	$h_K = 1.0$ mm
l_{SG}	SG length	$l_{SG} = 10.9$ mm *
l_K	SG length with clearance	$l_K = l_{SG} + c_{Cavity}$
l_C	sensor cavity length	$l_C = l_K + \frac{w_K - w_{KCC}}{2 \times \tan\alpha}$
n	number of wire cavities	$n = 2$
c_{Cavity}	clearance around the SG	$c_{Cavity} = 0.3$ mm
w_{CC2}	width of each wire cavity	$w_{CC2} = d_{wire} + 0.6$ mm
w_{dCC}	width of area between wire cavities	$w_{dCC} = 0.6$ mm
w_K	width of the cavity	$w_K = w_{SG} + c_{Cavity}$
w_{SG}	SG width	$w_{SG} = 5.9$ mm *
w_{KCC2}	front width of the sensor cavity	$w_{KCC2} = 2 \times w_{CC2} + 4 \times 0.3$ mm

concluded in the same study. It was shown that remelting a material can improve its surface roughness. This remelting of the surface was combined with an optimization of the PBF-LB/M upskin parameters for PureAl to achieve the lowest possible surface roughness. A surface roughness S_A of 12.6 µm could be achieved with single remelting, and could be reduced to a S_A of 11.8 µm with double remelting.

Even though these measures improved the surface roughness, the results demonstrated that mechanical preparation of the measurement surface remained necessary for PureAl parts. This mechanical preparation within the PBF-LB/M process chamber was performed using a rotary tool with an attached crystal fiber brush and various grits of sandpaper. The mechanically prepared bonding surface was visibly smoother, as could be seen with the naked eye (illustrated in Fig. 6).

Surface roughness was characterized using a VK-X3000 laser microscope (Keyence Corporation, Osaka, Japan). The measured S_a value of 3.4 µm indicates that the surface is well-suited for bonding with cyanoacrylate adhesives. Preliminary investigations showed that higher surface roughness can result in unreliable sensor signals. Additionally, the literature recommends avoiding surfaces with S_a values greater than 4 µm [19, 20].

The most reliable design for the wire cavity with the smallest necessary volume determined in this study consists of two separate wire cavities with a diameter w_{CC2} of 1.2 mm and an additional elongation of the teardrop-shaped cavity h_E of 0.9 mm. In all cases of ground faults in preliminary tests, the wire was damaged during the building process of the"roof" of the wire cavity. The use of two-wire cavities, one for each wire, allows for more reliable and repeatable positioning of the wire.

To quantify how well the integrated SG is encapsulated and protected from the environment, small test samples were built with a threaded bore to add a pneumatic connector. To fill the gap between the wire and its cavity, QPOX 90 (ATM Qness GmbH, Mammelzen, Germany) is applied. QPOX 90 is a cold-curing epoxy resin developed for metallographic cold-mounting. It cures in 24 h, has very low viscosity and is designed to fill small gaps and cracks [28]. A mass spectrometer (ASM 310, Pfeiffer Vacuum GmbH, Asslar, Germany) was utilized to evaluate the helium tightness of the sensor cavity by measuring the helium leak rate. The samples were pressurized with helium to 1.5 bar, and a sniffer probe was employed to detect any escaping helium. Out of six examined samples of the final cavity design, all showed leak rates around 1.8×10^{-6} mbar L s^{-1} to 2.3×10^{-6} mbar L s^{-1}, confirming their helium-tight sealing [29, 30]. Therefore, the design can be considered hermetically sealed.

With CC-33A identified as the optimal adhesive and the cavity design finalized, additional temperature tests were performed at the integration area using the presented configuration. During the initial temperature measurements (see Fig. 3), a build plate heating temperature of 60 °C resulted in a maximum temperature of 83 °C at the integration site. Given that the glass transition temperature of CC-33A is 150 °C, an additional safety margin of 5 °C was applied. To balance the requirement for build plate heating—critical for minimizing residual stresses—with the need to protect the SG and adhesive, the suitable plate heating temperature was calculated by adding the difference between 145 °C and 83 °C to the initial 60 °C. This adjustment led to the selection of a build plate heating temperature of 122 °C. Subsequent temperature tests using 122 °C build plate heating revealed that the maximum temperature at the integration site reached 143 °C, ensuring a 7 °C margin from the critical adhesive temperature. Exceeding this temperature could compromise process reliability. Thus, 122 °C will be maintained for future experiments and integration procedures.

3.4 Position of the integration and the process interruption

The optimal placement of sensor integration within a part is influenced by the geometry of the part, the dimensions of the sensor and wire cavities, and the expected mechanical loads. Ideally, the sensor is positioned as close as possible to the physical measuring quantity of interest, without weakening the mechanical properties of the part to a degree that would

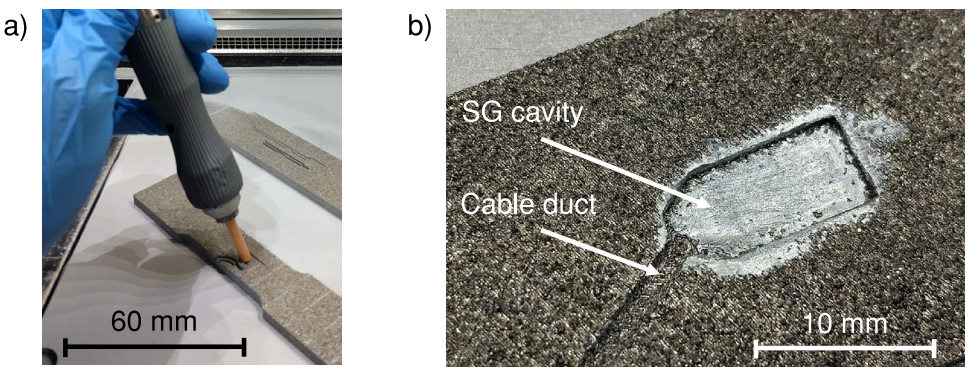

Fig. 6 Mechanical preparation of the bonding surface: (**a**) surface roughness improvement using a rotary tool, and (**b**) surface ready for SG integration

compromise its intended function. Besides preventing a mechanical failure, the position of integration needs to allow for the secure positioning of the SG wires by either having a horizontal wire cavity or by placing the wires downwards in the opposite direction of material build-up. In summary, the choice of the position of sensor integration is flexible, and mostly limited by the size of the SG and the minimum material thickness dependent on the load case. Figure 7 shows a schematic of the layer of interruption in regard to the sensor cavity. If the bottom of the wire cavity is designed to be on the same level as the bottom of the sensor cavity, the layer of process interruption directly influences the height of the insulating powder layer above the wires. The height from the bottom of the cavity to the layer of interruption h_{PI} should be as large as possible, while still leaving the sensor and wire cavity accessible for integration. Three possible positions for the layer of interruption exist. The interruption could occur during the build-up of the knee cavity, at the beginning of the roof build-up, or during the build-up of the roof. Since significant inaccuracies and formation of drops in the roof geometry of wire cavities with a roof angle γ of 55° were observed, it is not considered reasonable to place the interruption during the build-up of the sensor cavity roof with a roof angle β of 20°. During the mechanical preparation of the SG bonding surface, avoiding damage to the cavity walls proved challenging, especially when using a rotary tool. Consequently, this resulted in a locally increased powder layer thickness near the upper edges of the cavity walls after recoating and resuming the process, which in turn led to increased spatter formation. It was observed that this effect stopped occurring after the solidification of the first two layers of the second phase of the build job. To prevent this phenomenon from negatively impacting the unsupported roof geometry, it is recommended to position the layer of interruption during the build-up of the knee cavity walls, as seen in Fig. 7a. For the chosen knee cavity height of 1.0 mm in this study, a height of h_{PI} of 0.9 mm above the cavity floor was chosen to accommodate the two layers required to rebuild the unintended removed material.

3.5 Integration and procedure to resume build job

For the integration of the SG, an interruption of the PBF-LB/M process is required. Detailed guidelines for the recommended steps during the interruption and the manual integration of the SG are provided in the appendix. After the integration, the process must be resumed by recoating a new powder layer, during which the SG becomes covered with loose powder. Since most unsolidified powder materials exhibit electrically insulating properties, no ground faults occur [31]. If additional electrical insulation is required, a coating can be applied to the SG.

Research regarding the impact of process interruptions on the mechanical properties of PBF-LB/M parts is partly contradictory. A few studies found a decrease in mechanical properties [18, 32] but most studies describe no detectable influence of the interruption [10, 18, 33–35]. Binder [10] describes process interruptions as being critical or not critical, depending on the height of the build-job, the material used, the length of the interruption and several other factors. Most studies, using AlSi10Mg as powder material, generally showed no change in material properties because of a process interruption. These material properties include no changes to the microstructure, no influence on the mechanical parameters and no influence on the porosity for process interruptions below 16 h of interruption time, with or without an open process chamber, and with or without build plate heating [10, 18, 33–36].

To minimize the impact of the process interruption, it is important to ensure that the recoated powder layer matches the intended layer thickness of the build job. This step is critical due to the thermal shrinkage experienced by the built

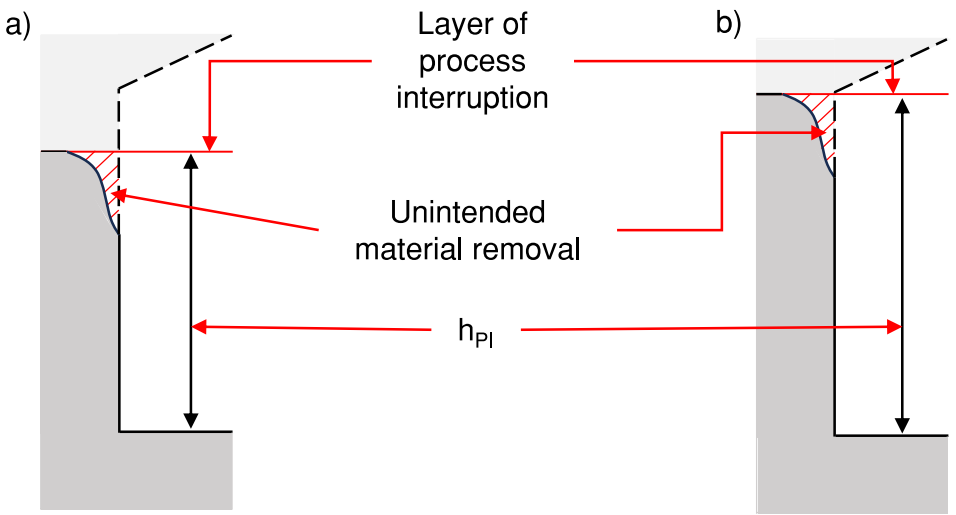

Fig. 7 Reasonable positioning of the layer of interruption: a) during build-up of the knee cavity, and b) at the beginning of the roof build-up

part as a result of the interruption. To reduce the effect of thermal shrinkage, the temperature difference caused by the interruption should be compensated. This can be achieved by heating the part to its equilibrium temperature using the build plate heating before restarting the process. A general heating time of 30 min is recommended if no direct measurement of the part temperature is possible. Based on Binder's findings [10], the thermal shrinkage, which occurs despite the heating provided by the build plate due to the part being preheated by the laser prior to the process interruption, can be approximately calculated. For an example sample height of h_b of 10 mm and a temperature difference of ΔT_u of 33 °C (between the part temperature before the interruption and after the interruption), the shrinkage is estimated to be roughly 0.10 mm. This value can be used to adjust the build plate upward by 0.10 mm before recoating a new powder layer. However, since this approximation by Binder [10] is a rough estimate and was based on AlSi10Mg instead of PureAl, a visual inspection is still recommended.

To know the exact position in z-direction of the integrated SG within the PBF-LB/M manufactured part, it is recommended to manufacture reference parts alongside the parts with integrated SG. A sample that is completed at the layer of interruption allows for the determination of the position of integration, measurable from the build plate. Two "arches" (Fig. 8) can be used to quantify the loss in build height resulting from the process interruption by comparing the reference dimension of an interrupted build to that of an uninterrupted one. Reference parts manufactured alongside the tensile specimens exhibited a height reduction of 0.2 mm due to the process interruption.

4 Validation

The measurement signal was analyzed using an extensometer UPM Zwick 50 kN (Zwick Roell GmbH & Co. KG, Ulm, Germany). The tensile sample was subjected to tensile forces ranging from 200 to 1000 N, applied in 200 N increments. Each load step was maintained for ten seconds. This stepwise test was conducted three times, with the sample being remounted between each test. The wires of the integrated SG were connected to a 1-SCM-SG350 adapter (HBK GmbH, Darmstadt, Germany), which was inserted into a QuantumX MX840B signal amplifier (HBK GmbH). This adapter converted the quarter-bridge configuration of the single SG into a full Wheatstone bridge. The signal amplifier was then connected to a computer running the catman analysis software (HBK GmbH).

Figure 9 displays the measurement results from the stepwise tensile test, showing the relative strain plotted over the test duration. The mean plots of the three tensile samples display highly similar trends. The nearly identical signal behavior and magnitude validate a successful SG integration, ensuring precise strain transfer from the measurement object. The high measurement precision confirms the validity of the integration methodology, including the selected adhesive and bonding surface preparation. Additionally, the cavity design was validated, as no ground fault was detected between the SG and the tensile specimen. It can also be concluded that the SG, wiring, and adhesive remained undamaged after the process resumed, despite exposure to laser energy and the resulting thermal impact.

To evaluate the validity of the SG measurements, strain data from Aramis (Carl Zeiss AG, Oberkochen, Germany), an optical strain measurement system, as well as readings from a conventional extensometer, were analyzed. However, both methods proved inadequate, as the local strain within the sensor cavity significantly exceeds the surface strain observed on the tensile specimen.

5 Conclusion and outlook

The methodical approach presented in this study successfully demonstrated the feasible integration of non-weldable SGs into PBF-LB /M components. By bonding an SG within a small sensor cavity using cyanoacrylate adhesive, measurements can be taken closer to the point of interest while offering enhanced protection for the SG against environmental influences compared to existing solutions. This innovative approach for monitoring strain loads in components requires minimal additional equipment and hardware beyond the standard PBF-LB /M manufacturing setup. Moreover, the methodology eliminates the need for long curing times, as the selected and recommended adhesive cures within just 60 s. The study also highlights that SG bonding is achievable even in the presence of powder within the process chamber.

For PureAl parts, a build plate heating of 122 °C and a process interruption height above the cavity floor h_{PI} of

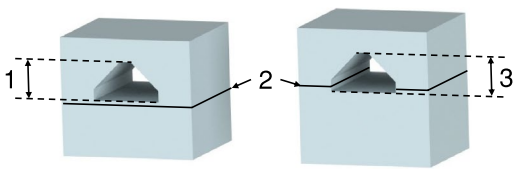

Pos. Nr.	Description
1	Reference dimension
2	Reference dimension with interruption
3	Process interruption

Fig. 8 Reference parts to determine the height loss caused by the process interruption

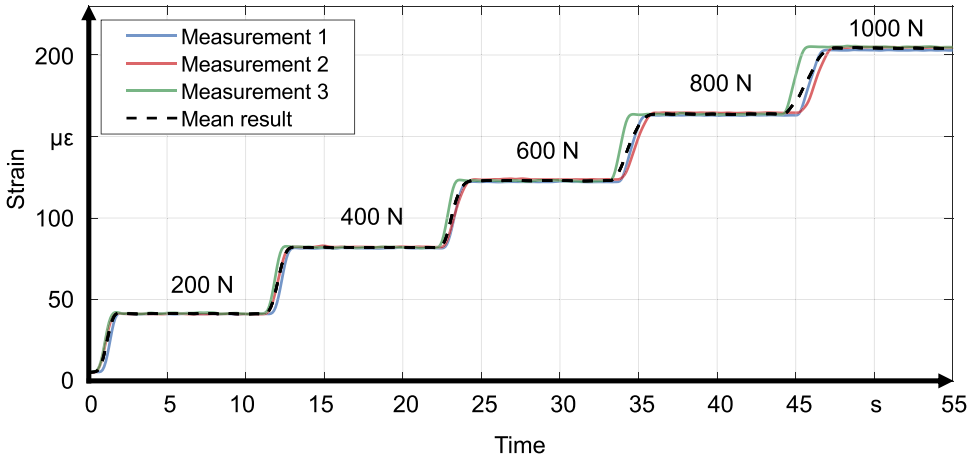

Fig. 9 Stepwise tensile test ranging from 200 to 1000 N, repeated three times (light, medium, and dark grey), with the mean of all measurement results represented by a dashed black line

0.9 mm are recommended, alongside the presented sensor and wire cavity geometries. The methodology developed in this study was validated through tensile sample testing, confirming its applicability under the specific boundary conditions, including the material and process parameters. It is assumed that the results are likely to be transferable to other metal powders for PBF-LB/M, other PBF-LB/M systems or other types of SG without significant effort. For example, applying this methodology to SG rosettes would necessitate changes to both the sensor and cable cavities, but the general principle of this method would remain largely unchanged. Applying this method to other PBF-LB/M systems or materials would likely result in different parameters for fabrication and different process temperatures.

Temperature measurements conducted at build plate heating levels of 60 °C and 122 °C indicate that the temperature at the position of integration is primarily determined by the build plate temperature, with only a minor influence from the applied laser parameters. These findings suggest that the integration of SGs may be feasible across a wide range of PBF-LB/M materials, including steels. Although higher melting points are not expected to significantly impact the local temperature at the position of integration, the effects of increased geometric complexity and reduced thermal conductivity in alternative powder materials require further investigation to ensure the applicability of the method under varying process and material conditions. Further studies should conduct a more detailed analysis of the signal quality and measurement accuracy of SGs integrated using this methodology and validate the approach by applying it to the use case of LIB cell housings to enable real-time monitoring.

Appendix

See Table 3.

Table 3 Appendix

Figure	Process Steps and Description	Tools and Equipment
	**Preparation of required tools and equipment:** Organize all required tools: SG, CC-33A, tweezers, Kapton tape, polyimide-foil, sandpaper K200 and K320, crystal fiber brush, rotary tool, cleaning swabs, scissors, ethanol, brush, powder sieve, cork, and PU140	See description
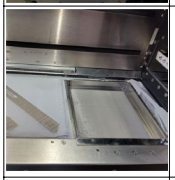	**Opening of process chamber:** • Open the process chamber after completing the first phase of the build job • Allow the build plate to cool to 60 °C to prevent exceeding the flash point of CC-33A of 75 °C • Lower powder supplier and insert powder sieve	Powder sieve
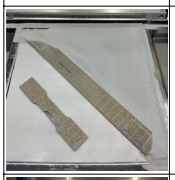	**Removal of powder:** • Remove powder from position of integration • Optional: Remove powder from build plate	Brush, vacuum cleaner
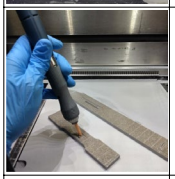	**Mechanical preparation of bonding surface:** • Finish the bonding surface using a rotary tool with a crystal fiber brush • Roughen the surface with K200 and K320 sandpaper grits • Ensure a surface roughness S_A of 2–4 µm	Rotary tool, crystal fiber brush, sandpaper K200 and K320
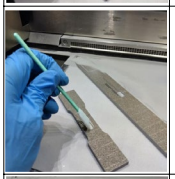	**Cleaning of surface:** • Remove grinding dust using a vacuum cleaner • Final cleaning step requires cleaning swabs that are resistant to snagging and abrading, ethanol or isopropanol	Vacuum cleaner, cleaning swab, ethanol or isopropanol
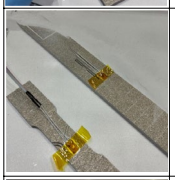	**Alignment of the SG:** • Preparation of SG by attaching a hinge-like tape on it • Align the SG within the cavity parallel to its side walls • Ensure rotational errors are minimized	SG prepared with Kapton tape
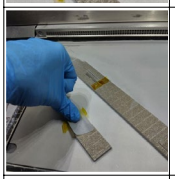	**Bonding the SG:** • Lift SG by using the tape-hinge • Apply CC-33A on measurement surface • Place a piece of polyimide foil on SG • Apply thumb pressure using a piece of to achieve uniform pressure and hold for 60 seconds	Polyimide foil, cork, CC-33A
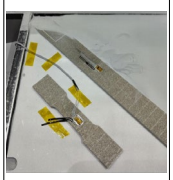	**Completing the sensor integration:** • Remove Kapton tape • Carefully press wires in their respective cavities using tweezers • If necessary for long wires, place them in the powder overflow and secure them using • Kapton tape and a weight • The wire has to stay flexible enough to allow for the movement of the build plate • Optional: apply PU140 as covering agent according to its instructions	Kapton tape, scissors, weights, PU140, tweezers
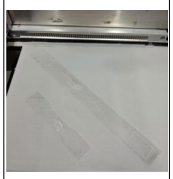	**Resuming the build job:** • Remove powder sieve and adjust the powder supplier to its previous level • Restart build plate heating • Once the target temperature is reached, allow 30 minutes for the component to heat thoroughly and for the PU140 to cure • Recoat powder and adjust the powder layer height of the first layer of the second phase of the build job • Restart without remelting	Powder material

Acknowledgements The authors would like to express their sincere thanks to Prof. Dr.-Ing. Rudiger Daub, Dr. Christoph Berger, and Kurt Hartmann for supporting this research. In addition, the authors would like to thank Jan Vochezer for his support.

Author contributions T.B. conceptualized the study, was project leader, and initally developed the Methodology. T.B. and N.F. wrote the main manuscript text and prepared the figures. All authors reviewed the manuscript. Additionally, C.S. acted as supervisor.

Funding Open Access funding enabled and organized by Projekt DEAL.

Data Availability No datasets were generated or analysed during the current study.

Declarations

Competing interests The authors declare no competing interests.

References

1. Feldmann S, Buchele R , Preveden V (2018) Predictive maintenance: from data collection to value creation, Roland Berger GmbH, Muenchen
2. Grand View Research Inc. (2023) Predictive maintenance market size and share report, 2030, URL https://www.grandviewresearch.com/industryanalysis/predictive-maintenance-market
3. Olajiga OK, Ani EC, Olu-lawal KA, Portillo Montero DJ, Adeleke AK (2024) Intelligent monitoring systems in manufacturing: current state and future perspectives. Eng Sci Technol J. https://doi.org/10.51594/estj/v5i3.870
4. Schmidt JP, Dandl S, Gentschev A-C, Elian K, Rose M (2016) Integrierte zell-sensorik in lithium-Ionen-akkus fuer elektro- und. hybridfahrzeuge. https://doi.org/10.1007/978-3-662-48944-4_1
5. AMA Fachverband fuer Sensorik e.V. (2014) Sensor-Trends 2014: Trends in zukunftsorientierten Sensortechnologien, ISBN: 978–3–642–01168–9, URL https://www.amasensorik.de/fileadmin/Pubikationen/AMA Trendbericht Langfassung[1].pdf
6. Edstroem K, Dominko R , Fichtner M , Perraud S (2022) Battery 2030+ Roadmap https://doi.org/10.33063/diva2-1452023.
7. Zhou L, Lai X, Li B, Yao Y, Yuan M, Weng J, Zheng Y (2023) State estimation models of lithium-ion batteries for battery management system: status, challenges, and future trends. Batteries 9(2):131. https://doi.org/10.3390/batteries9020131
8. Bareth T, Lehmann M, Schlick G, Seidel C (2024) Smart battery cell housings through additive manufacturing: potentials and challenges. Procedia CIRP. https://doi.org/10.1016/j.procir.2024.10.049
9. Binder M, Machnik A, Bosch M, Kreitz K, Schlick G, Seidel C (2022) In-situ integration of weldable strain gauges in components manufactured by laser-based powder bed fusion.
10. Binder M (2023) Integration von sensoren in additiv gefertigte metallbauteile (Dissertation). Technische Universitaet Muenchen
11. Binder M, Kirchbichler L, Seidel C, Anstaett C, Schlick G, Reinhart G (2019) Design concepts for the integration of electronic components into metal laser-based powder bed fusion parts. Procedia CIRP 81:992–997. https://doi.org/10.1016/j.procir.2019.03.240
12. Stoll P, Mathew J, Spierings A, Bauer T, Maier RRJ, Wegener K (2016) Embedding fibre optical sensors into. SLM Parts. https://doi.org/10.3929/ethz-a-010802374
13. Maier RRJ, Havermann D, MacPherson WN, Hand DP (2013) Embedding metallic jacketed fused silica fibres into stainless steel using additive layer manufacturing technology, in: L. R. Jaroszewicz (Ed.), Fifth European Workshop on Optical Fibre Sensors, SPIE Proceedings, SPIE, p. 87942U. https://doi.org/10.1117/12.2026076.
14. Havermann D, Mathew J, MacPherson WN, Maier RRJ, Hand DP (2015) Temperature and strain measurements with fiber bragg gratings embedded in stainless steel 316. J Lightwave Technol 33(12):2474–2479. https://doi.org/10.1109/JLT.2014.2366835
15. Warnck M, Binder M, Edelmann G, Fruechtl M, Taha I (2022) Condition monitoring of multi-material lightweight components through a sensitive outer skin using Fiber-Bragg-Grating sensors. Procedia CIRP 110:311–316. https://doi.org/10.1016/j.procir.2022.06.056
16. Binder M, Fischer M, Dietrich S, Seidel C, Reinhart G (2020) Integration of strain gauges in components manufactured by laser-based powder bed fusion, machining innovations conference for aerospace industry 20th https://doi.org/10.2139/ssrn.3724097.
17. Dani I (2019) Smart components by additive technologies. IOP Conf Ser Mater Sci Eng 480:012016. https://doi.org/10.1088/1757-899X/480/1/012016
18. Binder M, Leong C, Anstaett C, Schlick G, Seidel C, Reinhart G (2020) Effects of process interruptions on the microstructure and tensile properties of AlSi10Mg parts manufactured by Laser-Based Powder Bed Fusion. Procedia CIRP 94:182–187. https://doi.org/10.1016/j.procir.2020.09.035
19. Hoffmann K (1989) An introduction to measurements using strain gages. Hottinger Baldwin Messtechnik GmbH. https://doi.org/10.1111/j.1475-1305.2001
20. Keil S (2017) Technology and practical use of strain gages: With particular consideration of stress analysis using strain gages, Ernst & Sohn, Berlin Germany
21. Gebhardt A (2016) Additive Fertigungsverfahren: Additive Manufacturing und 3D-Drucken fuer Prototyping - Tooling - Produktion, 5th Edition, Hanser eLibrary, Hanser, Muenchen, https://doi.org/10.3139/9783446445390? locatt=mode:legacy.
22. Jiang X, Ye T, Zhu Y (2020) Effect of process parameters on residual stress in selective laser melting of AlSi10Mg. Mater Sci Technol 36(3):342–352. https://doi.org/10.1080/02670836.2019.1705560
23. Hottinger BK (2024) LS31HT weldable strain gauge for high temperatures
24. Hottinger BK (2024) Selection guide for strain gauges for experimental tests, last checked on 17.06.2024, URL https://www.hbkworld.com/en/knowledge/resource-center/articles/strainmeasurement-basics/strain-gauge-fundamentals/how-to-find-the-right strain-gauge.
25. Hottinger BK (2024) HBM shop, last checked on 28.07.2024, URL
26. Schimbaek D, Kaserer L, Mair P, Mohebbi MS, Staron P, Maier-Kiener V, Letofsky-Papst I, Palm F, Montes I, Hoeppel HW, Leichtfried G, Pogatscher S (2024) Advancements in metal

additive manufacturing: In-situ heat treatment of aluminium alloys during the laser powder bed fusion process. Mater Sci Eng, A 905:2018. https://doi.org/10.1016/j.msea.2024.146102
27. DaSilva LFM Handbook of adhesion technology, Springer Science+Business Media LLC, NewYork NY
28. ATM Qness GmbH, Cold Mounting, last checked on 09.10.2024, URL https://www.qatm.com/products/consumables/mounting/cold-mounting/.
29. Nolek, Helium leak detection basics, URL https://www.nolek.com/wpcontent/uploads/2018/02/Heliumleakdetectionbasics2018.pdf (2024).
30. Emrich N, Meyer SP, Daub R (2020) Ageing behavior of thermally joined hybrids of laser pre-treated metal and thermoplastic polymers, in: Proceedings of the 35th International Conference of the Polymer Processing Society (PPS-35), AIP Conference Proceedings, AIP Publishing, p. 020001. https://doi.org/10.1063/1.5142916.
31. Garino TJ (2002) Electrical behavior of oxidized metal powders during and after compaction. J Mater Res. https://doi.org/10.1557/JMR.2002.0389
32. Stoll P, Spierings A, Wegener K (2019) Impact of a process interruption on tensile properties of SS 316L parts and hybrid parts produced with selective laser melting. Int J Adv Manuf Technol 103(1–4):367–376. https://doi.org/10.1007/s00170-019-03560-1
33. Pouille Q, Ladaci A, Lomello F, Cheymol G, Laffont G, Lerner A, Maskrot H, Girard S, Aubry P (2022) Impact on mechanical properties following a process interruption during Additive Manufacturing. Procedia CIRP. https://doi.org/10.1016/j.procir.2022.08.032
34. Stokes RM, Yadollahi A, Priddy MW, Bian L, Hammond VH, Doude HR (2023) Effects of build interruption and restart procedure on microstructure and mechanical properties of laser powder bed fusion Al-Si-10Mg. J Mater Eng Perform 32(4):1576–1588. https://doi.org/10.1007/s11665-022-07217-1
35. Mahtabi MB, Yadollahi A, Stokes R, Doude YJHM, Bian L (2022) Effects of process interruption during laser powder bed fusion on microstructural and mechanical properties of fabricated parts. 10.26153/ tsw/44128.
36. Moser M, Brenner S, Strauss L, Loewisch G, NedeljkovicGroha V (2024) Effect of a process interruption on the mechanical properties of AlSi10Mg components produced by laser powder bed fusion (PBFLB/M). Prog Add Manuf. https://doi.org/10.1007/s40964-024-00641-w